The Journal of Chemical Physics

Steady-state free precession experiments and exact treatment of diffusion in a uniform gradient

Cite as: J. Chem. Phys. **115**, 4249 (2001); https://doi.org/10.1063/1.1389859
Submitted: 11 April 2001 . Accepted: 14 June 2001 . Published Online: 20 August 2001

D. E. Freed, U. M. Scheven, L. J. Zielinski, P. N. Sen, and M. D. Hürlimann


View Online

Export Citation

ARTICLES YOU MAY BE INTERESTED IN

Diffusion and field-gradient effects in NMR Fourier spectroscopy
The Journal of Chemical Physics **60**, 2966 (1974); https://doi.org/10.1063/1.1681477

Spin Diffusion Measurements: Spin Echoes in the Presence of a Time-Dependent Field Gradient
The Journal of Chemical Physics **42**, 288 (1965); https://doi.org/10.1063/1.1695690

Application of Fourier Transform Spectroscopy to Magnetic Resonance
Review of Scientific Instruments **37**, 93 (1966); https://doi.org/10.1063/1.1719961

AIP Publishing

© 2001 American Institute of Physics.

Steady-state free precession experiments and exact treatment of diffusion in a uniform gradient

D. E. Freed, U. M. Scheven, L. J. Zielinski,[a] P. N. Sen, and M. D. Hürlimann
Schlumberger-Doll Research, Old Quarry Road, Ridgefield, Connecticut 06877-4108

(Received 11 April 2001; accepted 14 June 2001)

We derive an analytic solution for the magnetization of spins diffusing in a constant gradient field while applying a long stream of rf pulses, which is known as the steady-state free precession (SSFP) sequence. We calculate the diffusion-dependent amplitude of the free induction decay (FID) and higher order echoes for pulses with arbitrary flip angle α and pulse spacing T_R. Stopped-SSFP experiments were performed in a permanent gradient field and the amplitudes of the first three higher order echoes were measured for a range of values of α and T_R. Theoretical results are in excellent agreement with experimental results, using no adjustable parameters. We identify various diffusion regimes in a rather large parameter space of pulsing and relaxation times, diffusion coefficient, and flip angle and discuss the interplay of the relevant time scales present in the problem. This ''phase diagram'' provides a road map for designing experiments which enhance or suppress the sensitivity to diffusion. We delineate the limits of validity of the widely used ansatz put forth by Kaiser, Bartholdi, and Ernst in their seminal paper. © *2001 American Institute of Physics.*
[DOI: 10.1063/1.1389859]

I. INTRODUCTION

Pulsed Nuclear Magnetic Resonance (NMR) is used for spectroscopy and imaging applications in a large number of fields, from physics and chemistry to medical imaging applications. One of the basic NMR techniques in use is steady-state free precession (SSFP),[1–3] where a periodic stream of rf pulses is applied to a sample that has been placed in a dc magnetic field. After some time the magnetization of the sample reaches a dynamic steady-state, giving rise to an NMR signal with the same periodicity as the applied rf sequence. The SSFP signal is more sensitive to diffusion and coherent spin displacements than a regular spin echo,[4] and therefore it has attracted considerable attention.

The purpose of this paper is threefold. First, we provide an exact analytical theory of SSFP for spins diffusing in an external constant magnetic field gradient. Second, we present experimental results and demonstrate quantitative agreement with the exact theory. Third, we use the exact theory to explore the behavior of magnetization in a rather large parameter space of various pulsing and relaxation times, diffusion coefficient and flip angle. This provides us with a deeper understanding of previous results in this area. We elaborate on these three themes—theory, experiment and exploration of the phase space—in the next few paragraphs.

Most work in this area, including ours, springs from the seminal work by Kaiser, Bartholdi and Ernst (KBE)[1] on the theoretical understanding of diffusion in SSFP in a linear magnetic field gradient. They described two methods of solution, one using a partition analysis of coherence pathways, and the other using a Fourier series decomposition of the steady-state magnetization. They suggested a simplifying ansatz that leads to a closed-form solution for the amplitudes of the Fourier modes. Their method is exact in the absence of diffusion and it is widely used. With diffusion, we will show that the KBE ansatz works well for some parameters, but it has limitations that give rise to large errors for parameters in the most diffusion sensitive regime. Carney *et al.*[5] calculated the coefficients of the Fourier series expansion for the FID and the first echo for pulsed field gradients and discussed results obtained for the special case of a tipping angle of 90°. They did not use the KBE-ansatz and confirmed their results with finite difference simulations of the Bloch-Torrey equation. Semiempirical approaches[6–8] as well as extensions of the KBE approach to pulsed gradient SSFP[9] have also been used. Discrepancies between theory and experiments have remained unexplained.[10,11]

The analytical solution obtained here in Sec. II starts with the Fourier decomposition of the magnetization, following the approach employed by KBE.[1] We derive a recursion relation for the Fourier coefficients, for which we obtain an exact analytical solution in terms of a continued fraction. This method allows us to understand the symmetry and convergence properties of the Fourier coefficients, and the limitations of the ansatz solution of KBE.[1] We also study the problem numerically using a finite difference method, in order to cross-check the analytical results. We find that the numerical approach gives identical results to the analytical solution. In Sec. IIA, we discuss the relevant time scales governing the diffusion physics and we delineate different regions of parameter space corresponding to different diffusion regimes. This serves as a ''qualitative'' guide for the rest of the paper to help understand the complex results more simply in terms of the various regimes of behaviors.

In Sec. III we proceed to present the results of stopped-SSFP experiments probing different diffusion regimes. The

[a]Also at Department of Physics, Harvard University, Cambridge, Massachusetts 02138.

 © 2001 American Institute of Physics

experiments consist of applying repeated rf pulses of flip angle α and period T_R to a phantom of water which has been placed in a permanent gradient field. When $T_2^* < T_R$, one observes NMR signals before and after every rf pulse. These signals are generated by refocused magnetization that has evolved over many different coherence pathways. When the pulsing is stopped, higher order echoes form at multiples of T_R, in place of the missing rf pulses. We show that these higher order echoes are highly diffusion sensitive. We measure the amplitude of the first three echoes for a wide range of α and T_R and find that our analytical solution (and the numerical simulations) are in excellent agreement with all experimental results, using no adjustable parameters. The experimental results thus validate our exact solution.

Next, the exact solution is used to understand *quantitatively* the diffusion sensitivity over a large range of parameter space. Section IV gives a quantitative illustration of different regimes and a comparison with previous theoretical solutions. This is particularly useful in designing and analyzing experiments where the sensitivity to diffusion can be large. We show that the higher echoes are especially sensitive to diffusion, much more than is suggested by the KBE-ansatz. These higher echoes have been observed not only in stopped-SSFP experiments, but also in the PFG-SSFP experiments used for fast imaging.[11,12]

The steady-state signal is more sensitive to diffusion than the spin echo because the steady-state signal has contributions from many different coherence pathways, while the spin echo is produced by a single coherence pathway. The other coherence pathways have, intrinsically, a higher diffusion sensitivity than the direct echo. A related effect of increased diffusion sensitivity has been recently analyzed for the CPMG sequence.[13] Under strong off-resonance conditions or for refocusing pulses different from 180°, other coherence pathways besides the direct echo start to contribute significantly to the observed echoes. This leads to an increased diffusion sensitivity of the signal.

II. TORREY EQUATION AND THE RECURSION RELATIONS

The setup of the problem and the initial development of the solution below follow closely that of Ref. 1. We write the coupled equations in a form whose structure extends beyond the example of the δ-function pulses considered in this paper.

We consider a system of spins in an externally applied magnetic field, $\vec{B}(\vec{r})$, with diffusion constant D and longitudinal and transverse relaxation times T_1 and T_2, respectively. Taking $\vec{B}(\vec{r})$ to point in the z-direction and to vary linearly in space with a gradient $\vec{g}$, we set $\vec{B}(\vec{r}) = (B_0 + \vec{g}\cdot\vec{r})\hat{\mathbf{z}}$. The offset of the Larmor frequency, $\Delta\omega_0$, is then given by $\Delta\omega_0(\vec{r}) = \gamma\vec{g}\cdot\vec{r}$, where γ is the gyromagnetic ratio. In SSFP we repeatedly apply an rf pulse characterized by a flip angle α, amplitude $\omega_1 = \gamma B_1$, and frequency $\omega_{\rm rf} = \gamma B_0$ with spacing T_R between pulses until steady-state is reached. In this paper we will assume the pulses to be instantaneous and ignore any diffusion and relaxation effects during the pulse. We will furthermore assume the pulses to be ''on resonance,'' that is, we will restrict our analysis to the case when $\Delta\omega_0(\vec{r}) \ll \omega_1$. Between the pulses, the transverse magnetization $M_{xy}(\vec{r},t) \equiv M_x(\vec{r},t) + iM_y(\vec{r},t)$ and the longitudinal magnetization $M_z(\vec{r},t)$ obey Bloch's equation, as modified by Torrey to include diffusion:[14]

$$\begin{aligned}\frac{\partial M_{xy}(\vec{r},t)}{\partial t} &= D\nabla^2 M_{xy}(\vec{r},t) - i\gamma\vec{g}\cdot\vec{r}M_{xy}(\vec{r},t) \\ &\quad - \frac{M_{xy}(\vec{r},t)}{T_2}, \\ \frac{\partial M_z(\vec{r},t)}{\partial t} &= D\nabla^2 M_z(\vec{r},t) - \frac{(M_z(\vec{r},t) - M_0)}{T_1}.\end{aligned} \tag{1}$$

A factor of $\exp(-i\omega_{\rm rf}t)$ has been divided out of $M(\vec{r},t)$ for clarity.

We define the precession angle (in the rotating frame) during time T_R by

$$\theta(\vec{r}) \equiv \gamma(\vec{g}\cdot\vec{r})T_R = \Delta\omega_0(\vec{r})T_R.$$

The spectrum of the steady-state signal is periodic in θ. This can be seen by the following simple argument. Changing the rf frequency of the pulses by any multiple of $2\pi/T_R$ will not change the effect of the pulses on the spins as long as the offset is small compared to ω_1. Obviously, it also does not affect the spins in any way between the pulses, while they precess and undergo diffusion. It follows that for translationally invariant systems, the magnetization in the rotating frame of the spins is a periodic function in θ.

Following Ref. 1, we can write the general solution of Eq. (1) for unrestricted diffusion in a constant gradient as a Fourier series

$$M_{xy}(\theta,t) = i\sum_{p=-\infty}^{\infty} b_p\, e^{i(p+t/T_R)\theta} E_{2,p}(t); \tag{2}$$

and

$$M_z(\theta,t) = M_0(1 - e^{-t/T_1}) + \sum_{p=-\infty}^{\infty} z_p\, e^{ip\theta} E_{1,p}(t), \tag{3}$$

where p is an integer, and

$$\begin{aligned}E_{2,p}(t) = \exp\{&-t/T_2 - D\gamma^2 g^2 T_R^3[p^2(t/T_R) + p(t/T_R)^2 \\ &+ \tfrac{1}{3}(t/T_R)^3]\}\end{aligned} \tag{4}$$

and

$$E_{1,p}(t) = \exp\{-t/T_1 - D\gamma^2 g^2 T_R^3 p^2(t/T_R)\}. \tag{5}$$

Equations (2) and (3) describe the evolution of the magnetization between rf pulses for each mode. In the mode expansion of Eqs. (2) and (3), the spatial dependence, or equivalently, the frequency dependence, is all contained in the phase factors $e^{i(p+t/T_R)\theta}$ and $e^{ip\theta}$ for the transverse and longitudinal modes, respectively. These factors show that the pth-modes of both M_z and M_{xy} immediately after a pulse are characterized by a spatial wave vector $\vec{k}_p = p\,\gamma\vec{g}\,T_R$. Between pulses the wave vectors remain constant for the longitudinal modes, but increase linearly from $\vec{k}_p$ to $\vec{k}_{p+1}$ for the transverse modes. The terms $E_{2,p}(t)$ and $E_{1,p}(t)$ describe the attenuation for each mode due to relaxation and diffusion

between the pulses. Both T_1 and T_1 relaxation are independent of the wave vector and identical for all modes. For unrestricted diffusion, the rate of diffusive attenuation of mode p is proportional to the square of the instantaneous wave vector $\vec{k}_p(t)$, and thus the mode decays as exp $[-\int_0^t dt' k_p^2(t')]$. With $\vec{k}_p(t)=(p+t/T_R)\,\gamma\vec{g}\,T_R$ for transverse modes and $\vec{k}_p(t)=p\,\gamma\vec{g}\,T_R$ for longitudinal modes, we obtain the diffusion-dependent terms in Eqs. (4) and (5), respectively. The presence of terms proportional to p^2 demonstrates that higher modes are intrinsically more sensitive to diffusion. At this point it is useful to introduce the diffusion time T_D defined by $D\gamma^2 g^2 T_R^3 \equiv T_R/T_D$.

The amplitude of the different transverse modes, b_p, can be easily separated experimentally based on the phase factors in Eq. (2). In a stopped-SSFP experiment, the wave vector for modes with $p<0$ will vanish at a time $|p|T_R$ after the last pulse. If $T_2^*<T_R$, this will lead to a series of distinct echoes with an amplitude $b_p E_{2,p}(|p|T_R)=b_p \exp\{-|p|T_R/T_2 - 1/3|p|^3 T_R/T_D\}$. The signal of mode $p=0$ is often referred to as the FID signal, and the signal for the mode $p=-1$ as the pre-FID signal. When $T_2^*>T_R$, the signals of the different modes interfere and give rise to the strong θ dependence of the SSFP signal first observed by Carr.[3] In this case, the different modes can be separated by phase cycling, as demonstrated by Zur *et al.*[15]

Now that we have described the evolution of the magnetization between rf pulses for each mode, we next turn our attention to the mixing of modes by the rf pulses. The rf pulses rotate some of the longitudinal magnetization into the transverse plane and vice versa. An rf pulse along the x-axis with angle α acting on the magnetization (M_{xy},M_z) yields the new transverse magnetization $M_{xy}(1+\cos\alpha)/2+M_{xy}^*(1-\cos\alpha)/2-iM_z\sin\alpha$ and longitudinal magnetization $-i(M_{xy}-M_{xy}^*)(\sin\alpha)/2+M_z\cos\alpha$. Thus, a pulse acting on magnetization of mode p generates magnetization of both mode p and $-p$.

The evolution between two successive pulses couples neighboring modes $p-1$ and p, and the rf pulse couples modes p and $-p$. Over n cycles, this leads to a coupling of all modes between $-n$ and $+n$. The coupling strength can be varied by changing the pulse angle α. In steady state, the amplitude of the lowest modes, b_0 and b_1, corresponding to the FID and pre-FID signals, will be affected differently by diffusion depending on how strongly the mode is coupled to the higher modes that have increased diffusion sensitivity.

To compute the mode amplitudes z_p and b_p for steady state, we substitute Eqs. (2) and (3) into the steady-state condition, $\vec{M}(\theta,0^-)=\vec{M}(\theta,T_R)$, where $\vec{M}(\theta,0^-)$ is the magnetization immediately before the application of a pulse. Equating the pth modes gives a recursion relation between the amplitudes b_p, b_{-p}, and b_{p-1}.

Taking advantage of the symmetries of Eq. (1) and of the rotation properties of rf pulses along the $\hat{x}$ axis, we see that if (M_{xy},M_z) is a steady-state solution for θ, then $(-M_{xy}^*,M_z)$ is a solution for $-\theta$. Since the Fourier expansion is unique, we can set them equal, which implies directly that the amplitudes b_p and z_p are real for all values of p and that $z_p=z_{-p}$.

With these symmetry properties, the resulting recursion relations for the amplitudes of the Fourier modes of the transverse magnetization, b_p, can then be written as:

$$A_p b_p - B_p b_{-p} - E_{2,p-1} C_p b_{p-1} = 0 \tag{6}$$

$$-B_p b_p + A_p b_{-p} - E_{2,-p-1} C_p b_{-p-1} = 0, \tag{7}$$

when $p>0$, and

$$(A_0-B_0)b_0 - E_{2,-1} C_0 b_{-1} = -\sin\alpha\, M_0(1-E_{1,0}), \tag{8}$$

when $p=0$. The coefficients A_p, B_p, and C_p are given by

$$A_p = \tfrac{1}{2}(E_{1,p}-1)(1+\cos\alpha) \tag{9}$$

$$B_p = \tfrac{1}{2}(E_{1,p}+1)(1-\cos\alpha) \tag{10}$$

$$C_p = (E_{1,p}-\cos\alpha) = A_p + B_p, \tag{11}$$

where $E_{1,p}\equiv E_{1,p}(T_R)$ and $E_{2,p}\equiv E_{2,p}(T_R)$. From a complete solution of the amplitudes b_p, the amplitudes of the Fourier modes of the longitudinal magnetization, z_p, can then be directly obtained from

$$z_p = \frac{\sin\alpha}{2C_p}(b_p + b_{-p}) \tag{12}$$

for $p\neq 0$, and

$$z_0 = \frac{\sin\alpha}{C_0} b_0 - \frac{M_0(1-E_{1,0})}{C_0} \tag{13}$$

for $p=0$. With the identification $z_0=c_0+M_0$ and $z_p=c_p/2$ for $p>0$, these recursion relations become identical to those in Eq. (20) in Ref. 1.

The correct analytical solution to these recursion relations is discussed in Sec. IIB. We want to point out here that the form of the coupled Eqs. (6)–(8) remains the same when off-resonance or shaped pulses are considered or when time-dependent gradients are used. Only the expressions for the coefficients A_p, B_p, C_p and the pulse transition element, $\sin\alpha$, will change. Thus, once we have a method for solving this set of coupled equations, it will apply to much more general cases. In the more general case, however, the mode amplitudes will be complex.

A. Diffusion regimes

Before discussing the general solution of the recursion relation, it is worthwhile to give a qualitative outline of different regimes into which the solutions fall.

In the presence of diffusion, the SSFP magnetization depends on the interplay of the flip angle, α, and the relative duration of the four relevant times, the relaxation times T_1 and T_2, the pulse repetition time T_R, and the diffusion time $T_D\equiv 1/(D\gamma^2 g^2 T_R^2)$ introduced above. For some values of the parameters, the FID or echoes have little or no dependence on diffusion, while for others they are quite sensitive to diffusion. Here we will identify the different regimes and summarize the leading behaviors. This will provide a framework for the discussion of our results in the following sections. Some of the limits have been discussed before,[1] while others will be studied in more detail in a later paper.

There are four regimes where we expect a reduced dependence on diffusion. The first regime is, (i) the *slow-*

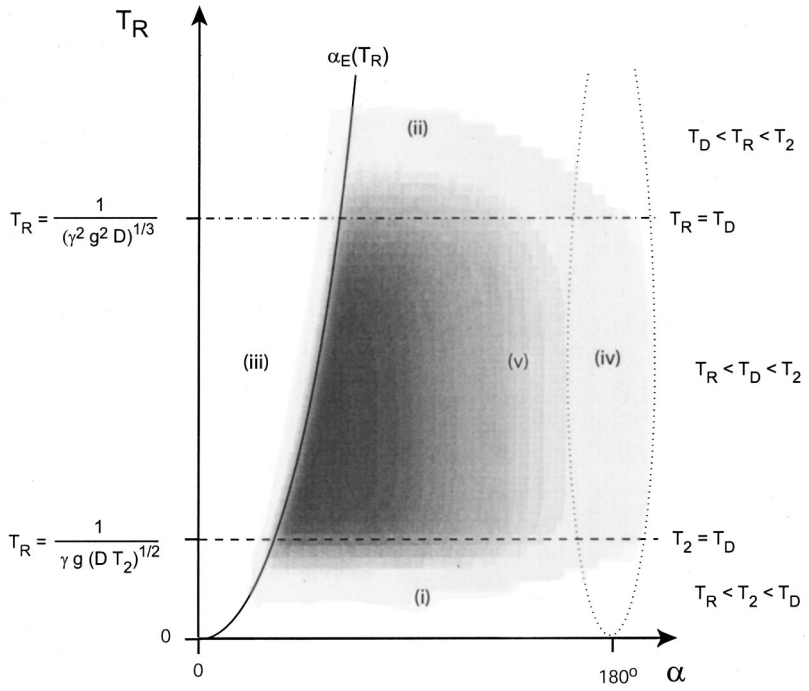

FIG. 1. Diffusion regimes for SSFP in the parameter space of flip angle α vs repetition time T_R. Regime (i) is the slow-diffusion or very-rapid-pulsing regime, regime (ii) is the fast-transverse-decay regime, regime (iii) is the small-flip-angle regime, and (iv) is the 180° flip-angle regime. Regime (v) is shaded and shows the strongest diffusion sensitivity.

diffusion regime or *very-rapid-pulsing regime* when $T_2 \ll T_D$. In this regime, the effect of diffusion on the lower modes is greatly reduced. This occurs for fast enough pulsing when the pulsing rate $1/T_R$ satisfies $1/T_R \gg \gamma g \sqrt{DT_2}$. For the higher modes p, this condition becomes $1/T_R \gg p\,\gamma g \sqrt{DT_2}$.

The second regime is, (ii) the *fast-transverse-decay regime* when T_R is longer than either T_D or T_2. In both these cases, the transverse magnetization decays almost completely in the time between the pulses and coherence is lost between each pulse. The FID signal is then dominated by coherence pathways that do not generate any transverse magnetization prior to the last pulse and are independent of diffusion. The amplitudes of all higher modes are strongly attenuated and are dominated by the shortest coherence pathways. For this reason, b_p for $|p| \geqslant 1$ depends on diffusion like $\exp\{-|p|T_R/T_{2\,\mathrm{eff}}\}$, where the effective relaxation time $1/T_{2\,\mathrm{eff}}(p)$ is given by[1]

$$1/T_{2\,\mathrm{eff}}(p) = 1/T_2 + p^2/(3T_D). \tag{14}$$

Thus, as p becomes larger, the echoes become more sensitive to diffusion. However, even in the absence of diffusion, the amplitudes of the higher modes are minuscule in this regime.

The third regime is, (iii) the *small-flip-angle regime* for the $p=0$ mode. It occurs when the flip angle α is less than the Ernst angle, α_E, where $\cos\alpha_E \equiv \exp(-T_R/T_1)$. In this case, the probability that the rf pulses refocus the spins or move them from the x-y plane to the z-axis and back again is small enough that again only the shortest coherence pathways (which have the minimal number of spin flips or refocusing) contribute significantly to the FID and the other echoes. Most of the magnetization is in the lowest longitudinal mode, z_0. The amplitude of the FID, b_0, scales like α/α_E and is to first-order independent of T_2 and diffusion. To leading order in α, the amplitudes of the higher modes scale like α/α_E for $p>0$ and like $(\alpha/\alpha_E)^3$ for $p<0$. Diffusion attenuates the higher modes again like $\exp\{-|p|T_R/T_{2\,\mathrm{eff}}\}$ with the effective relaxation time given by Eq. (14).

Finally, the fourth regime is, (iv) the 180° *flip-angle regime* when the angle α is close to 180°. In this case, the transverse magnetization is effectively refocused by every pulse. Most of the magnetization will remain in the $p=0$ and $p=\pm 1$ modes, without exciting any higher modes. This is similar to the situation in the Carr-Purcell Meiboom-Gill (CPMG) sequence,[16,17] where the signal is refocused by a series of 180° pulses. Because the spins never sample the higher modes, the FID and first echo will have a limited dependence on diffusion. In this regime, the diffusion sensitivity can be taken into account by replacing T_2 in the calculation without diffusion by the effective relaxation time $1/T_{2\,\mathrm{eff}} = 1/T_2 + 1/(3T_D)$.

We expect higher diffusion sensitivity in the parameter space (v) between these four regimes, which is shown shaded in Fig. 1. This occurs at intermediate pulse repetition rates. The slow-diffusion or very-rapid-pulsing regime (i) is below the dashed line. The fast-transverse-decay regime (ii) is above the dashed-dotted line. The small flip-angle regime (iii) is to the left of the solid line that indicates the Ernst angle as a function of pulse spacing, $\alpha_E(T_R)$. We indicate the fourth regime, the 180° flip-angle regime (iv), schematically as the dotted area around $\alpha = 180°$. The diffusion-sensitive region (v) only exists if the slow-diffusion regime (i) and the fast-transverse-decay regime (ii) do not overlap. The condition can be written as

$$\gamma^2 g^2 D\, T_2^3 > 1. \tag{15}$$

Equation (15) shows that a Hahn echo with pulse spacing T_2 must be significantly attenuated by diffusion. In this case, regime (i) is characterized by $T_R < T_2 < T_D$, regime (v) by

$T_R<T_D<T_2$, and regime (ii) by $T_D<T_R<T_2$. Otherwise, if Eq. (15) is not fulfilled, relaxation will always dominate diffusion.

Figure 1 shows the four regimes with reduced diffusion sensitivity for the FID. This figure is meant to be a qualitative road map for a large phase space. Specific quantitative examples are given in Figs. 2–5 and additional ones for imaging applications will be published elsewhere.

Diagrams for the higher order echoes are similar to Fig. 1, except that region (iii) is missing and the line separating regime (i) and (v) is shifted down by a factor of $1/p$. For the higher modes with $|p|>0$, smaller pulse angles will lead to higher diffusion sensitivity within the regime (v). Buxton[10] first pointed this out based on an analysis of the dominant coherence pathways and their diffusion sensitivity. In the absence of diffusion, small angles generate transverse magnetization that have relatively more contributions at higher modes compared to the magnetization generated by higher pulse angles. Diffusion affects these higher modes more strongly, leading to an enhanced diffusion sensitivity for smaller pulse angles. In general, the presence of higher order echoes for $D=0$ indicates that higher modes are populated and well-coupled to the lower modes. This leads to enhanced diffusion sensitivity.

B. Solution of the recursion relations

In this section, we discuss the solution for the mode amplitudes b_p for general values of diffusion, pulse angle, and the four relevant time scales. It is based on solving the recursion relations for b_p given in Eqs. (6)–(8). From the complete set of amplitudes for the transverse modes, b_p, the amplitudes for the longitudinal modes, z_p can then be obtained directly from Eqs. (12) and (13).

If we know one of b_0 or b_{-1}, we can solve Eq. (8) for the other one. Once we have both b_0 and b_{-1}, we can compute all the other Fourier coefficients b_p by repeated applications of Eqs. (6) and (7). To see this more clearly, we begin by rewriting Eqs. (6) and (7) as

$$b_p=\frac{1}{A_p}[E_{2,p-1}C_p b_{p-1}+B_p b_{-p}], \tag{16}$$

and

$$b_{-p-1}=\frac{1}{E_{2,-p-1}A_p}[-E_{2,p-1}B_p b_{p-1} +(A_p-B_p)b_{-p}]. \tag{17}$$

Then, for example, if b_0 and b_{-1} are known, Eq. (16) can be used to obtain b_1 and Eq. (17) to obtain b_{-2}. Once these are known, the process can be repeated to find b_2 and b_{-3}, and so on. All that is lacking for obtaining the full solution is the value of b_0 or b_{-1} or some combination of the two.

Thus, in order to compute the entire hierarchy of the Fourier coefficients b_p in Eqs. (6)–(8), we need one additional condition on these coefficients. It is determined by the physical requirement that the magnetization $M(\theta,t)$ be finite for arbitrary values of θ and t. To this end we must impose the boundary condition "at infinity" by requiring that the mode amplitudes b_p go to zero as $p\to\pm\infty$.

The implementation of this boundary condition requires some care. Based on physical arguments, it is clear that the amplitudes of the higher modes, corresponding to high wave vectors, will become smaller as the magnitude of the wave number is increased. In the absence of diffusion, the decay of b_p versus p is in fact exponential[1] with a decay rate that is identical for the positive and negative modes. In the presence of diffusion, we expect an even faster decay.

In Ref. 1, it was assumed that with diffusion the decay rate of the positive modes is still identical to the decay rate of the negative modes, i.e., $b_{|p|}/b_{|p|-1}=b_{-|p|-1}/b_{-|p|}$. This assumption is in general incorrect.

In solving the recursion relations, it is essential to retain the proper coupling between the modes with positive and negative mode number $\pm|p|$, as they are directly coupled by the rf pulses. For this reason, it is advantageous to introduce the ratios

$$r_p\equiv-\frac{b_{-p}}{b_{p-1}}. \tag{18}$$

We note that if we can solve for $r_1=-b_{-1}/b_0$, then, according to the above discussion, we can solve for the amplitudes of all the modes.

The ratios r_p follow a recursion relation given by

$$r_p=\frac{E_{2,p-1}C_p}{B_p}\left[1-\frac{A_p^2}{E_{2,-p-1}C_pB_pr_{p+1}+A_p^2-B_p^2}\right]. \tag{19}$$

This equation is obtained by taking the ratio of Eqs. (16) and (17) with p replaced by $-p$ and eliminating r_{p+1} from the numerator. According to Eq. (17), we can obtain a relation between the amplitudes of two adjacent modes b_{-p-1} and b_{-p} for $p\neq0$ in terms of r_p:

$$b_{-p-1}=\frac{1}{E_{2,-p-1}A_p}\left(E_{2,p-1}B_p\frac{1}{r_p}+(A_p-B_p)\right)b_{-p}. \tag{20}$$

In the absence of diffusion, the recursion relation connecting r_p and r_{p+1}, Eq. (19), does not have any p dependence and r_p becomes a constant, independent of p. Equation (20) then shows that the mode amplitudes b_p form a geometric series, i.e., they decay exponentially in $|p|$.

In the presence of diffusion, r_p becomes dependent on p and, therefore, there is no longer a fixed relationship between the corresponding positive and negative modes. This can be seen as follows. The boundary condition for b_{-p} at $p=+\infty$ implies that for large p the modes must decay. We can always find mode numbers p larger than any given number such that $|b_{-p-1}|<|b_{-p}|$. Since $E_{2,-p-1}$ approaches zero with increasing $|p|$, Eq. (20) shows that this boundary condition can only be fulfilled if, for large p, the ratio r_p approaches

$$r_p=-\frac{E_{2,p-1}B_p}{A_p-B_p}. \tag{21}$$

This expression shows that in the presence of diffusion, r_p goes to zero as $p\to\infty$. This implies that the amplitudes with negative mode numbers, $b_{-|p|}$, decrease faster with $|p|$ than those with positive mode numbers, $b_{|p|-1}$.

Note that Eq. (19) relates r_p to r_{p+1}. In keeping with the boundary conditions, we can set r_{l+1} to zero for some large number l and use Eq. (19) to solve for r_l. Then we can substitute r_l into the right-hand side of Eq. (19) to find r_{l-1}. This process can be repeated until the solution for r_1 is obtained. This solution for the ratio r_1 is a continued fraction. To express this solution in the standard continued fraction notation, we begin by letting

$$r_1=\frac{1}{E_{2,-1}B_{p=0}}x_1+\frac{E_{2,0}C_{p=1}}{B_{p=1}}. \tag{22}$$

The truncated continued fraction is given by

$$x_1=\cfrac{n_1}{d_1+\cfrac{n_2}{d_2+\cfrac{n_3}{d_3+\ldots\cfrac{n_l}{d_l+e_l}}}}, \tag{23}$$

where the numerator, n_p, is given by

$$n_p=-E_{2,-p}E_{2,p-1}A_p^2B_{p-1}/B_p, \tag{24}$$

the denominator, d_p, is given by

$$d_p=(A_p-B_p)+E_{2,-p-1}E_{2,p}B_pC_{p+1}/B_{p+1}, \tag{25}$$

and the extra term is given by

$$e_p=-E_{2,p}E_{2,-p-1}B_pC_{p+1}/B_{p+1}. \tag{26}$$

The exact solution is the continued fraction obtained by taking $l\rightarrow\infty$. This continued fraction converges for all values of the diffusion coefficient D.

Since this continued fraction converges very quickly, it is possible to truncate it at a mode number l that is only slightly larger than the highest mode number of interest. Truncation at a mode number l corresponds to setting $r_{l+1}=0$, as mentioned above, and setting the mode amplitude $b_{-l-1}=0$. In our calculations, we found that truncation at $l=5$ or 6 results in mode amplitudes for the first few modes that are accurate to several decimal places.

Using the truncated continued fraction, Eq. (23), we can then compute r_1 to any desired accuracy by choosing the appropriate truncation limit l. Substituting $b_{-1}=-r_1b_0$ into Eq. (8), we can immediately compute the lowest mode amplitudes, b_0 and b_1:

$$\begin{aligned} b_0&=\frac{-\sin\alpha\, M_0(1-E_{1,0})}{A_{p=0}-B_{p=0}+E_{2,-1}C_{p=0}r_1},\\ b_{-1}&=-r_1b_0. \end{aligned} \tag{27}$$

As explained above, the amplitudes of all the higher modes can then be simply obtained by repeatedly applying Eqs. (16) and (17). If the continued fraction has been truncated at $p=l$, then the solution for the modes will be accurate until p approaches l.

C. Finite difference solution

A finite difference solution of Eq. (1) under a SSFP was performed to double-check the recursion solution outlined above. The numerical procedure used is a simple extension of that given in Refs. 18 and 19 to include a term for M_z as in Eq. (1). This term was not present in Refs. 18 and 19, where a CPMG sequence with perfect, on-resonance 180° pulses was considered.

We consider diffusion along the x- axis inside a cell of size L_S that is subdivided with a step size $\Delta x=L_S/(N-1)$, such that the jth position is at $x_j=(j-1)\Delta x$, $j=1,\ldots N$. The time is subdivided with a step size Δt, such that $[1/T_2+4D/(\Delta x^2)]\Delta t=2$. We consider reflecting boundary conditions at $x=0$ and $x=L_S$. By taking a sufficiently large container, these numerical solutions can be directly compared with those obtained by the recursion analysis. For numerical stability, we use the unconditionally stable Cranck-Nicholson procedure. This procedure is similar to those used previously by others in another context (see for example, Ref. 20).

In between pulses, we solve two diffusion equations, one for $M_{xy}(t)$ which includes transverse relaxation T_2 and the precession in the magnetic field gradient, and another for the longitudinal $M_z(t)$ component without any precession but with T_1 relaxation. The initial values are given by the magnetization at the end of the previous pulse. For $M_{xy}(t)$, we combine the time evolution matrix for diffusion and phase rotation in a single microstep, and, using the Cranck-Nicholson[20] method, we find the time evolution matrix U for a single micro-time-step Δt. This gives the lattice version of $\exp(-i\gamma B\Delta t/2)\exp[-\Delta t/(2T_2)]\exp(\Delta tD\nabla^2)\exp(-i\gamma B\Delta t/2)\exp[-\Delta t/(2T_2)]$. To obtain the evolution for the entire period between pulses, we raise this matrix to a power given by the number of microsteps in between two pulses. Similarly, the evolution for the $M_z(t)$ component is given by the lattice version of $\exp[-\Delta t/(2T_1)]\exp(\Delta tD\nabla^2)\exp[-\Delta t/(2T_1)]$ and so forth. At the end of diffusive periods, the rf pulse mixes $M_{xy}(t)$ and $M_z(t)$ components as described above. Then the procedure is repeated.

The entire procedure is repeated for a time period equal to several times T_1 when a steady state is reached. We find that over the whole range of parameters, the numerical results of the finite difference solution and of the recursion relation can be made identical within the desired accuracy.

III. EXPERIMENTS

A. Experimental procedure

To test the theoretical analysis, we performed stopped steady-state free precession measurements in the fringe field of a superconducting magnet. This somewhat unusual mode of operation was chosen because we had available to us an NMR probe operating at 1.76 MHz for geophysical applications, and because measurements in the fringe field obviate the need for quasistatic pulsed field gradients. Our measurements permit the simultaneous measurement of the SSFP signal on and off-resonance. The off-resonance results will be discussed elsewhere. Note that the diffusion and NMR physics explored in this work do not depend on the Larmor frequency, except through the well known field dependence of T_1 and T_2.

The sample was placed at a location with a field strength of 41.5 mT and a uniform static field gradient of 131 mT/m. The sample was a 12.3 mM solution of water doped with NiCl to give a measured $T_2=48.1$ ms and a diffusion coefficient $D=2.3\times10^{-9}$ m^2/s. Note that at such low fields $T_1=T_2$. The cylindrical sample cell (2 cm$\times$3.14 cm^2) was placed in the center of a comparatively large solenoid coil (10 cm$\times$12.5 cm^2), ensuring adequate rf homogeneity. The experiments were conducted for a range of rf power settings and pulse spacings. The pulses were 25 μs long and had amplitudes corresponding to flip angles between 0° and 180°. The repetition times between subsequent pulses, T_R, were in the range of 1 to 3 ms. The dead time of our NMR probe is on the order of Q/f, which in our case was about 50 μs.

To establish the steady-state, pulse trains were applied for a duration of 160 ms$=3.3\,T_1$. After this time the pulsing was stopped abruptly. Distinct echoes form at times where the next pulses would occur and are well-separated in time, with typical echo widths on the order of the pulse durations. We acquired the first three echoes. The echoes were each Fourier-transformed and the same phase corrections applied to the entire data set. Here we only discuss the near-resonance component of the signals, i.e., when $\Delta\omega_0 \ll \omega_1$ and the rf pulses rotate magnetization around an axis in the transverse plane.

The three acquired echoes correspond to the modes $p=-1$, -2, and -3, respectively. According to Eq. (2), the respective amplitudes are $b_{-1}E_{2,-1}(T_R)$, $b_{-2}E_{2,-2}(2T_R)$, and $b_{-3}E_{2,-3}(3T_R)$.

In order to eliminate all adjustable parameters, separate experiments were performed to establish the value of the equilibrium magnetization M_0 and the relaxation time T_2 to better than 1% accuracy. The values of the flip angles were calibrated separately as well, limiting the systematic error for the flip angles to less than two degrees.

With our experimental parameters, we can probe four of the five regimes that we have identified in Sec. III.A. We have chosen a sample with a fairly short relaxation time to allow efficient data averaging, but long enough that the condition of Eq. (15) is still well-fulfilled. For the two repetition times of $T_R=1$ and 3 ms, the corresponding values for the diffusion time T_D are 344 and 40 ms, respectively. Thus, using the measured value $T_2=48.1$ ms, our experiments were probing the slow diffusion regime (i) with $T_D \gg T_2$ for $T_R=1$ ms, and an intermediate to fast diffusion regime (v) where $T_D \leqslant T_2$ for $T_R=3$ ms. The corresponding Ernst angles are $\alpha_E=11.6°$ and $\alpha_E=20.0°$, and our experiments extend over all flip angle regimes discussed in Sec. II.A.

B. Comparison of theory, experiments and numerical simulation

In this section we compare the three approaches discussed in this paper: The theoretical calculations based on the Fourier mode expansion, the numerical solutions with finite-difference simulations, and experimental results of the stopped steady-state experiments. In Fig. 2 we compare the amplitudes of the first, second, and third echoes as a function of flip angle α for the parameters previously discussed.

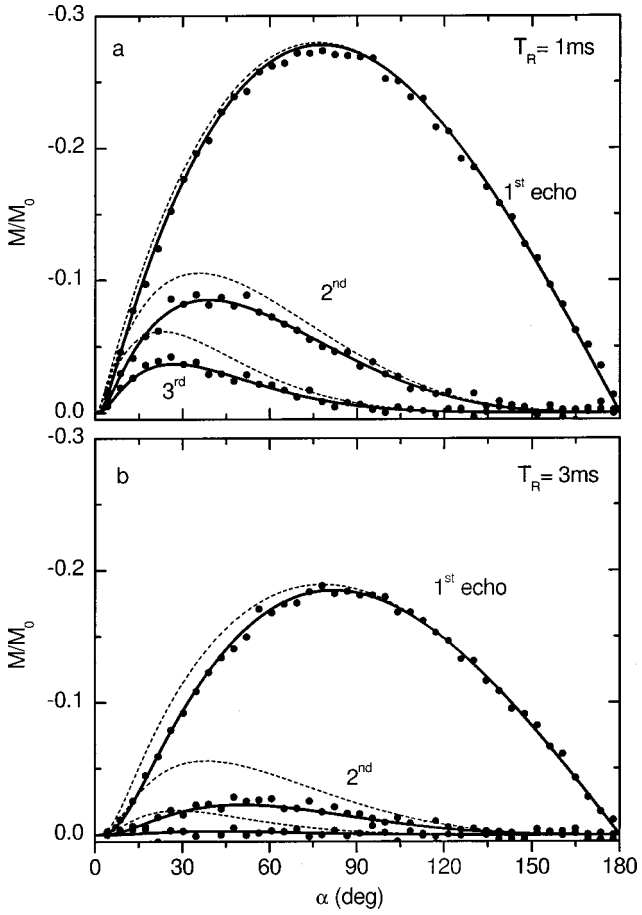

FIG. 2. Comparison of our analytical solution (solid) with stopped-SSFP experiments (dots), vs flip angle α. We plot the first three echo amplitudes corresponding to modes $p=-1$, -2, and -3, respectively. The data are obtained with a doped water phantom ($T_2=48.1$ ms), for repeat times T_R of 1 and 3 ms in Figs. a and b, respectively. The plot demonstrates excellent agreement of our theory and experiment. The theory of Ref. 1 (dashed) is shown for comparison.

The results of the analytical calculation and numerical simulation fall on top of each other and are shown as solid lines. The experimental data are shown as circles. The agreement is excellent for all echoes and over the full range of angles and repetition times T_R studied. Note that there are no adjustable parameters.

The dashed lines in Fig. 2 indicate the analytical solution given in Ref. 1. In the literature, this solution has often been used as a theoretical reference. There are clear discrepancies between that approach and our theory and measurements. As discussed in Section II.B, the deviations are caused by the incorrect assumption made in Ref. 1 relating the decays of the negative and positive modes. This leads to an incorrect coupling between the higher modes when diffusion is important.

IV. QUANTITATIVE ILLUSTRATION OF DIFFERENT REGIMES AND COMPARISON WITH PREVIOUS THEORETICAL SOLUTION

It is instructive to analyze the discrepancy between the two theoretical approaches further, because it identifies the parameter space where diffusion and coupling to higher

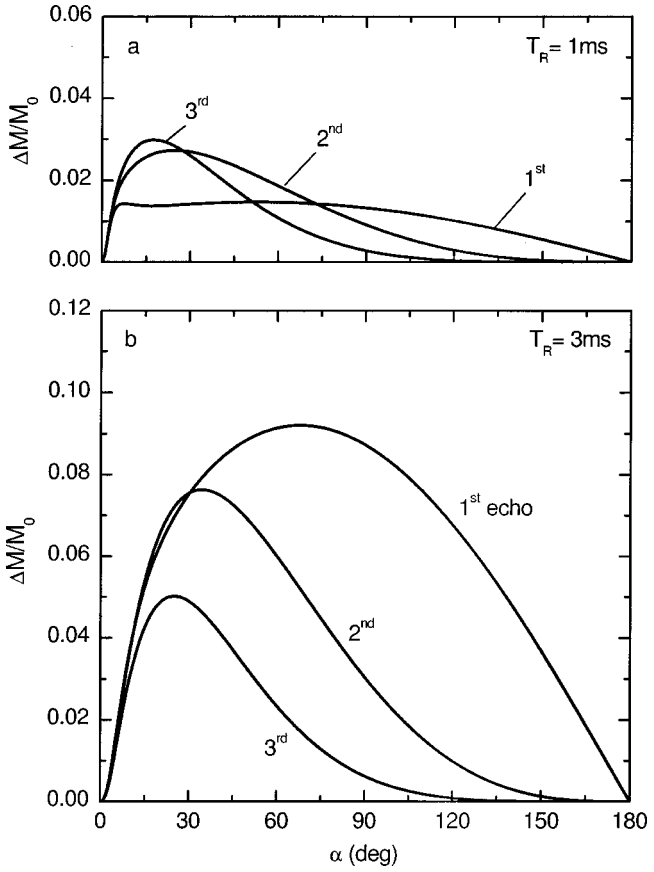

FIG. 3. Diffusive signal loss $\Delta M/M_0$ vs flip angle α, for the first three echoes. We calculate the signal in the presence and in the absence of diffusion, and plot the difference of the two, for parameters corresponding to the experimental results depicted in Fig. 2. Figure 3a ($T_R=1$ ms, $T_D>T_2$) illustrates that in the fast pulsing regime the diffusive attenuation is comparatively small. Note that the diffusion effects are smaller for low modes and hence the 1st echo is less affected by diffusion than the 2nd and 3rd. Figure 3b ($T_R=3$ ms, $T_D\leqslant T_2$) depicts the diffusion sensitive regime, with large diffusive attenuation for all echoes.

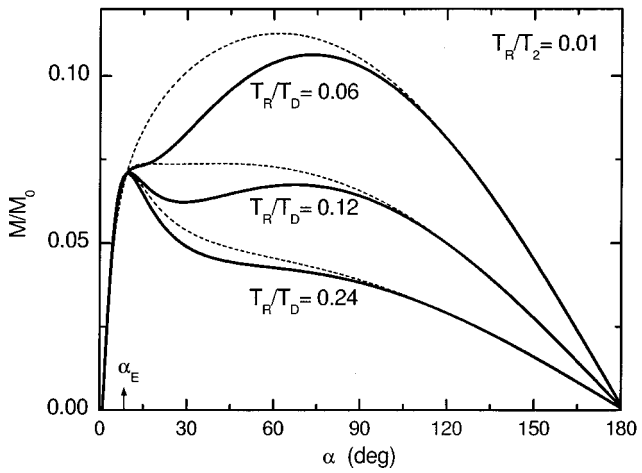

FIG. 4. Calculated FID amplitude (solid lines) vs flip angle α for three values of the diffusion parameter $T_R/T_D=Dg^2\gamma^2T_R^3$, in the regime where $T_R<T_D<T_2$. In the small-flip-angle regime ($\alpha<\alpha_E$) diffusion effects are small and vanish at α_E. For angles above α_E, diffusion becomes important. For intermediate flip angles, coupling to higher order modes gives rise to enhanced diffusion sensitivity when compared to the ansatz solution (dashed lines) by Ref. 1.

modes is important. For $T_R=1$ ms, the results for the first echo show only minor differences in Fig. 2a. In this case, $T_D>T_2$ and we are in regime (i). Diffusion is not of great importance for the first echo and the two theoretical approaches agree. The higher echoes are more sensitive to diffusion and show a more pronounced disagreement.

With the parameters of Fig. 2b, $T_D<T_2$ and we are probing regimes (v) and (iv). Here we can see that even for the first echo, the previous theoretical calculation in Ref. 1 is noticeably inaccurate for angles less than about 100°. At higher angles, we are entering regime (iv), where only the first two modes are effectively coupled. This can also be seen by the fact that the amplitudes of the higher modes become very small. In this range, the incorrect coupling to the higher modes in Ref. 1 has no consequence for the calculation of the amplitude of the first echo. However, notice that at smaller angles the discrepancy for the higher echoes becomes very pronounced.

A. Diffusion sensitivity of the first three echoes

The diffusion sensitivity of the data shown in Fig. 2 is studied more explicitly in Fig. 3. Here we show the calculated differences in echo amplitudes for $D=0$ and $D=2.3\times10^{-9}$ m^2/s, the value of the diffusion coefficient of water relevant for our experiments. This corresponds to the diffusion contrast of the measurements. This figure confirms that the contrasts are much smaller in regime (i), represented in Fig. 3a, than in regime (v), represented in Fig. 3b.

Note that in the slow diffusion regime (i) and for angles less than about 75°, the diffusion contrast is larger for the higher echoes than for the first echo, even though the overall echo amplitudes decrease with echo number. This confirms that the higher echoes are much more sensitive to diffusion.

B. Diffusion sensitivity of the FID

We now turn our attention to the diffusion sensitivity of the FID, i.e., of the mode with $p=0$. In our present experimental setup in the fringe field, we were not able to measure this mode because its signal decays within a time of the order of the pulse width, i.e., 25 μs. This is within the dead time of our instrument.

We concentrate on the regime of intermediate repetition time T_R, where $T_R<T_D<T_2$. This range of parameters shows the strongest diffusion sensitivity and is described by regimes (iii), (iv), and (v) shown in Fig. 1. For our illustration in Fig. 4, we have chosen longer relaxation times, $T_1=T_2$, than in our experiments to make the intermediate T_R region much wider and avoid ''end effects'' from the other regimes.

At angles below the Ernst angle, we are in the small-flip-angle regime [regime (iii)]. The amplitude of the FID increases linearly with flip angle and is insensitive to diffusion. At the Ernst angle, the FID signal is completely independent of diffusion. This follows directly from Eq. (8), since at the Ernst angle $C_{p=0}=0$ and the amplitude of the FID becomes $b_0(\alpha_E)=M_0\sin\alpha_E/(1+\cos\alpha_E)$, independent of diffusion and T_2 relaxation.

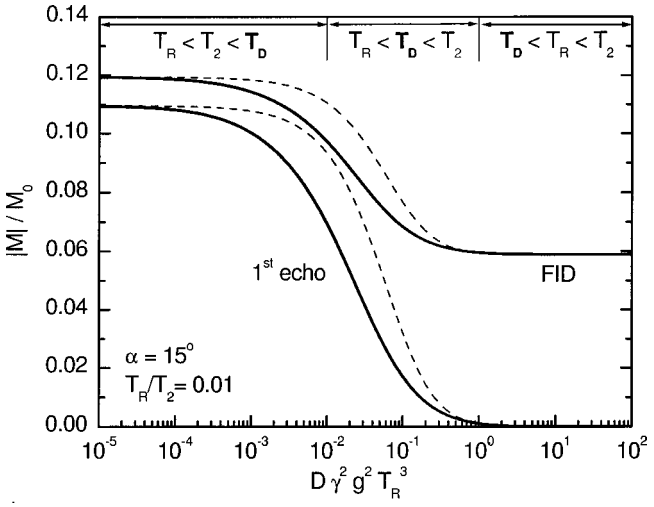

FIG. 5. Magnitude of the FID and the first echo (solid lines) vs the diffusion parameter $T_R/T_D = Dg^2\gamma^2 T_R^3$, for fixed T_R. For very small diffusion ($T_D \gg T_2$) the magnitudes of the FID and first echo are asymptotically independent of diffusion. In the intermediate regime the diffusion sensitivity is pronounced, differing substantially from the solution of Ref. 1. For very large diffusion $T_D \ll T_R$ the first echo asymptotically goes to zero, while the FID approaches a diffusion independent amplitude.

At angles above the Ernst angle, we reach the diffusion-sensitive regime (v). In this regime, Fig. 4 confirms that the FID amplitude is a strong function of the diffusion coefficient and the amplitudes calculated for the three different diffusion coefficients clearly separate. The results in Fig. 4 also reveal that the angle dependence can be more complicated than was previously known. For certain diffusion coefficients, the angle dependence shows two local maxima. Such behavior is caused by the interplay of diffusion and T_2 relaxation, and cannot be generated if the loss of coherence is solely due to T_2 relaxation.

Comparison with the dashed lines shows that the KBE ansatz[1] used before is not able to describe this diffusion sensitive region accurately. The discrepancy in amplitude can exceed 20% and has prevented the extraction of accurate diffusion information in previous SSFP experiments.[10] For angles larger than approximately 120°, the behavior is described by the large angle regime (iv), and the previous theoretical description is adequate, as expected.

C. Extraction of the diffusion coefficient from the data

A more direct illustration of the diffusion sensitivity of the FID and the first echo is shown in Fig. 5. We display the magnitudes of these signals versus diffusion coefficient, with all other parameters kept constant. We chose a flip angle $\alpha = 15°$ that is larger than the Ernst angle, $\alpha_E = 8.1°$. This enables us to probe the diffusion sensitive regime. The repetition time T_R is chosen to be much shorter than the relaxation times: $T_R/T_1 = T_R/T_2 = 0.01$.

For very small diffusion coefficients, the diffusion time T_D is very long and exceeds both T_2 and T_R. This situation is described by the slow diffusion regime (i). As the diffusion coefficient is increased, T_D becomes shorter. When T_D approaches T_2, the diffusion sensitive regime (v) is reached. Diffusion becomes important and leads to a decrease of the observed amplitudes. If the diffusion coefficient is further increased, so that T_D becomes even shorter than T_R, all transverse magnetization is lost between pulses. The amplitudes of the first and higher echoes vanish, whereas the amplitude of the FID becomes $b_0 = M_0 \times \sin\alpha(1-\exp\{-T_R/T_1\})/(1-\cos\alpha\exp\{-T_R/T_1\})$, independent of diffusion. In this fast-transverse-decay regime (ii), the asymptotic FID amplitude has only contributions from pathways that do not generate transverse magnetization prior to the last pulse.

If the SSFP sequence is used to estimate the diffusion coefficient of the sample, the operating parameters should be chosen such that the experiment probes the steepest part of the curve in Fig. 5, i.e., probes the diffusion-sensitive regime (v). Comparison with the ansatz used in the previous theoretical solution[1] shows again a large discrepancy exactly in this regime. In order to extract an accurate diffusion coefficient from the measured amplitudes, it is essential to use our full solution. The ansatz will lead to an error in the estimated diffusion coefficient that can exceed 50%.

V. CONCLUSION

In this paper we study the effects of diffusion on SSFP both theoretically and experimentally. We find excellent quantitative agreement between theory and experiment with no adjustable parameters. Prior studies reported only qualitative agreement.

We make a comprehensive study over a broad range of parameters, including the relaxation times T_1, T_2, the diffusion time T_D, the pulse repeat time T_R, and the flip angle α. We demonstrate that the results can be classified into different diffusion regimes and identify the parameter space that generates signals with the highest diffusion sensitivity. Exploring the broad range of parameter space gives not only a quantitative understanding of the various regimes but also insight into prior work and the physics of growth and decay of signals.

The nature of the coupling among the various Fourier modes is affected strongly by diffusion. Due to this effect, the KBE ansatz, which assumes that the amplitudes of Fourier modes with positive and negative mode number p decay in the same way versus p, breaks down. This leads to significant deviations in the regime of the parameter space that is most sensitive to diffusion. The ansatz also becomes inaccurate for the higher echoes in all regions of parameter space. On the other hand, the KBE ansatz works well when diffusion effects are small or when only the lowest modes are populated. This includes the following regimes: slow-diffusion regime ($T_2 \ll T_D$), fast-transverse-relaxation regime ($T_R > T_D$ or $T_R > T_2$), small-flip-angle regime ($\alpha < \alpha_E$) and 180° flip-angle regime. For small flip angles, the FID is shown to be first linearly proportional to the flip angle and then to deviate strongly from the KBE ansatz as the flip angle exceeds the Ernst angle.

The map of the different diffusion regimes should aid in designing experiments. The pulse spacings and angles can be chosen to heighten the diffusion sensitivity in order to mea-

sure the diffusion coefficient or to obtain diffusion-weighted images. In addition, even though the higher order echoes have lower signal intensity than the FID,[11,12] they are more sensitive to diffusion and may be exploited for increased diffusion contrast.[11] Alternatively, the pulse spacings and other parameters can be chosen to minimize the effects of diffusion so that the measurements are essentially independent of diffusion.

Although we have presented here only the simplest example of a steady-state sequence, the principles involved are very general. In fact, more complicated sequences, such as those with pulsed-field gradients or shaped rf pulses, can be explained within the framework set forth in this paper. In particular, the rf pulses serve to mix the various modes. In this paper, changing the angle of the pulses affects the amount of mixing. Variations such as having shaped pulses, off-resonant pulses, or a sequence of several pulses that repeat, only change the amount of mixing between the modes. We will address these other types of sequences in another paper. Variations such as adding a pulsed-field gradient modify the evolution of the modes between pulses in a straightforward way. Thus, our explanation of the simple, on-resonant SSFP sequence also forms the basis for understanding these more complex sequences.

ACKNOWLEDGMENTS

The authors are grateful to Scott Axelrod for useful discussions. Work at Harvard was supported in part by NSF DMR 99-81283.

[1] R. Kaiser, E. Bartholdi, and R. R. Ernst, J. Chem. Phys. **60**, 2966 (1974).
[2] R. Bradford, C. Clay, and E. Strick, Phys. Rev. **84**, 157 (1951).
[3] H. Y. Carr, Phys. Rev. **112**, 1693 (1958).
[4] S. Patz and R. C. Hawkes, Magn. Reson. Med. **3**, 140 (1986).
[5] C. E. Carney, S. T. S. Wong, and S. Patz, Magn. Reson. Med. **19**, 240 (1991).
[6] P. Waldstein and W. E. Wallace, Rev. Sci. Instrum. **42**, 437 (1971).
[7] K. D. Merboldt, W. Hänicke, M. L. Gyngell, J. Frahm, and H. Bruhn, J. Magn. Reson. **82**, 115 (1989).
[8] D. Le Bihan, R. Turner, and J. R. Macfall, Magn. Reson. Med. **10**, 324 (1989).
[9] E. X. Wu and R. B. Buxton, J. Magn. Reson. **90**, 243 (1990).
[10] R. B. Buxton, Magn. Reson. Med. **29**, 235 (1993).
[11] C. T. Mizumoto and E. Yoshitome, Magn. Reson. Med. **18**, 244 (1991).
[12] D. J. Kim and Z. H. Cho, Magn. Reson. Med. **19**, 20 (1991).
[13] M. D. Hürlimann, J. Magn. Reson. **148**, 367 (2001).
[14] H. C. Torrey, Phys. Rev. **104**, 563 (1956).
[15] Y. Zur, M. L. Wood, and L. J. Neuringer, Magn. Reson. Med. **16**, 444 (1990).
[16] H. Y. Carr and E. M. Purcell, Phys. Rev. **94**, 630 (1954).
[17] S. Meiboom and D. Gill, Rev. Sci. Instrum. **29**, 688 (1958).
[18] P. N. Sen, A. André, and S. Axelrod, J. Chem. Phys. **111**, 6548 (1999).
[19] L. J. Zielinski and P. N. Sen, J. Magn. Reson. **147**, 95 (2000).
[20] G. P. Zientara and J. H. Freed, J. Chem. Phys. **72**, 1285 (1980).